RSC Advances

PAPER

View Article Online
View Journal | View Issue

Check for updates

Cite this: *RSC Adv.*, 2022, **12**, 3561

Facile synthesis of g-C_3N_4 quantum dots/graphene hydrogel nanocomposites for high-performance supercapacitor†

Di Liu, Tran Van Tam and Won Mook Choi *

This work demonstrates a facile one-pot method for preparing graphitic carbon nitride (g-C_3N_4) quantum dots/graphene hydrogel (CNQ/GH) nanocomposites using a hydrothermal process, in which graphene sheets of a graphene hydrogel (GH) are decorated with g-C_3N_4 quantum dots (CNQDs) and have a 3D hierarchical and interconnected structure through a typical self-assembly process. The obtained CNQ/GH nanocomposite demonstrates improved electrochemical performances of a supercapacitor with a specific capacitance of 243.2 F g^{-1} at a current density of 0.2 A g^{-1}. In addition, the fabricated symmetric supercapacitor (SSC) using CNQ/GH electrodes exhibits a high energy density of 22.5 W h kg^{-1} at a power density of 250 W kg^{-1} and a superior cycling stability with a capacitance retention of 89.5% after 15 000 cycles. The observed improvements in the electrochemical performance of CNQ/GH electrodes are attributed to the large surface area with abundant mesopores and various C–N bonds in CNQDs, which promote efficient ion diffusion of electrolyte and electron transfer and provide more active sites for faradaic reactions. These obtained results demonstrate a facile and efficient route to develop potential electrode materials for high-performance energy storage device applications.

Received 10th December 2021
Accepted 16th January 2022

DOI: 10.1039/d1ra08962e

rsc.li/rsc-advances

Open Access Article. Published on 27 January 2022. Downloaded on 2/8/2026 1:35:48 PM.
This article is licensed under a Creative Commons Attribution-NonCommercial 3.0 Unported Licence.

Introduction

Supercapacitors have received great attention as one of the efficient energy storage devices for powering electronics due to their high power capability, long cycling stability and low maintenance costs.[1–3] Based on the charge storage mechanism, supercapacitors can be classified as electric double-layer capacitors (EDLCs) and pseudocapacitors. Various electrode materials such as activated carbon, carbon nanotubes, and graphene have been studied extensively for use in EDLCs.[4–10] Among them, graphene as a two-dimensional monolayer of sp^2-hybridized carbon atoms is attracting constant attention due to its outstanding features such as large surface area, high electrical conductivity, and good durability.[11–13] In particular, graphene hydrogel (GH) is a three-dimensional (3D) porous network of graphene sheets that is considered as a potential active material for supercapacitors because of its high porosity, large specific surface area and high electrical conductivity.[14–16] The highly porous structure of GH facilitates electrolyte penetration, thereby exposing most graphene sheets to the electrolyte. However, the non-faradaic charge storage mechanism in these graphene-based materials causes limited specific capacitance.

Graphitic carbon nitride (g-C_3N_4) is another suitable active material for use in supercapacitors in virtue of its chemical stability, nitrogen-rich framework, environmental-friendly characteristics, and mild synthesis conditions.[17–23] Among these features, high N content of g-C_3N_4 can provides active sites for faradaic reactions and increases the surface polarity to enhance wettability to electrolyte and mass transfer efficiency, resulting in improved electrochemical performance. In particular, the incorporation of pyrrolic and pyridinic N group in g-C_3N_4 can be favorable for improving the pseudocapacitance.[24,25] In this regard, g-C_3N_4 quantum dots (CNQDs), a novel zero-dimensional g-C_3N_4 with ultrasmall size less than 10 nm, can be used as supercapacitor electrodes, which is ascribed to abundant surface functional groups of CNQDs for access of electrolyte ions and large surface area for efficient ion transportation of electrode.[26] In addition, the well-developed nanostructures and abundant active sites by high N content could lead to achieve enhanced electrochemical performances. However, there are few reports on the use of CNQDs as electrodes for supercapacitors.[26]

Herein, we report a facile one-pot preparation route of CNQDs decorated GH nanocomposites (denoted as CNQ/GH) for the electrode materials of symmetric supercapacitors. The hydrothermal reaction was carried out using graphene oxide (GO) and CNQDs mixture solution to obtain CNQ/GH nanocomposites, showing a 3D hierarchical and interconnected structure of graphene sheets decorated with CNQDs. Moreover, the CNQDs could effectively attach on graphene sheets *via* π–π

School of Chemical Engineering, University of Ulsan, 93 Daehak-ro Nam-gu, Ulsan 44610, Republic of Korea. E-mail: wmchoi98@ulsan.ac.kr

† Electronic supplementary information (ESI) available. See DOI: 10.1039/d1ra08962e

© 2022 The Author(s). Published by the Royal Society of Chemistry

Open Access Article. Published on 27 January 2022. Downloaded on 2/8/2026 1:35:48 PM.
This article is licensed under a Creative Commons Attribution-NonCommercial 3.0 Unported Licence.

interaction. The incorporation of CNQDs onto the graphene sheets of porous GH network can improve ion diffusion and transport capability at the electrode–electrolyte interface and enhance the faradaic reaction, leading to the enhanced specific capacitance. The obtained CNQ/GH nanocomposites exhibited a higher specific capacitance than that of the GH electrode. In addition, the assembled symmetric supercapacitor using CNQ/GH electrodes showed a high energy density and good cycling stability.

Experimental details

Preparation of CNQDs

First, 5 g of melamine was calcined in a muffle furnace at 550 °C for 4 h to synthesize bulk g-C_3N_4, which was then treated with a mixture of concentrated sulfuric acid and nitric acid for approximately 2 h at room temperature. After the solution mixture was washed several times with deionized (DI) water, a white product of porous bulk g-C_3N_4 was obtained. Then, the mixture suspension of 400 mg of the obtained porous bulk g-C_3N_4 and 100 mL of concentrated aqueous NH_3 solution was prepared and transferred into a 200 mL Teflon-lined autoclave, which was heated at 180 °C for 12 h to prepare porous g-C_3N_4 nanosheets. Next, 10 mg of the obtained porous g-C_3N_4 nanosheets were dispersed in 100 mL of DI water, followed by ultrasonicating the mixture for 6 h. The resulting aqueous suspension mixture was centrifuged at 7000 rpm and dialyzed using a dialysis tube (3000 Da, Spectrum Lab. Inc.) against DI for 2 days to obtain CNQDs.

Preparation of CNQ/GH nanocomposites

CNQ/GH nanocomposites were obtained according to the procedure described in our previous report.[27] In briefly, 125 mL of a homogeneous aqueous solution of GO (Standard Graphene Co., GO-4401) at a concentration of 2.5 mg mL^{-1} containing different amount of CNQDs was transferred into a 200 mL Teflon-lined autoclave and heated at 180 °C for 12 h. After cooling to room temperature, the product was collected and freeze-dried to obtain CNQ/GH. The prepared nanocomposites were designated as CNQ*X*/GH, where "*X*" denote the added amount of CNQDs (1, 3, and 5 wt%). For comparison, GH without CNQDs was also prepared by the same procedure using GO solution only.

Characterizations

Scanning electron microscopy (SEM) images and energy dispersive spectrometry (EDS) mapping images were acquired with a JEOL FESEM-JSM820, and transmission electron microscopy (TEM) images and high-resolution transmission electron microscopy (HRTEM) images were obtained using a Hitachi H-8100 TEM instrument. X-ray diffraction (XRD) measurements were performed using a Bruker D8 Advance diffractometer with non-monochromated Cu Kα radiation operating at 40 kV and 30 mA. Fourier transform infrared (FTIR) spectra were obtained using a Nicolet IR 200 FT-IR spectrometer (Thermo Scientific). X-ray photoelectron spectroscopy (XPS: Thermo Fisher) measurements were performed using monochromatic AlKα radiation ($h\nu = 1486.6$ eV).

Electrochemical measurements

Electrochemical characteristics of the prepared CNQ/GH nanocomposites were investigated using cyclic voltammetry (CV), galvanostatic charge/discharge (GCD), and electrochemical impedance spectroscopy (EIS) measurements. All electrochemical measurements were performed using a Bio-Logic VSP electrochemical workstation at room temperature. A three-electrode system was used to test the electrochemical performance of the prepared electrodes with Pt wire and Ag/AgCl electrodes as counter and reference electrodes, respectively. The working electrode was prepared by mixing the obtained CNQ/GH nanocomposites, acetylene black and polyvinylidene fluoride (PVDF) in *N*-methyl-2-pyrrolidone (NMP) in a mass ratio of 80 : 10 : 10. The as-prepared slurry mixture was coated onto the surface of the glass carbon electrode (5 mm in diameter), with an average mass loading of about 0.5 mg cm^{-2}, and then dried at 40 °C for 1 h in an oven. All electrochemical tests were performed in an aqueous electrolyte of 6 M KOH at room temperature. EIS studies were performed at open circuit potential in a frequency range from 10 kHz to 0.01 Hz with AC amplitude of 5 mV.

Fabrication of all-solid-state symmetric supercapacitor (SSC)

Ni foam as a current collector was first pressed under a pressure of 10 MPa and washed several times with acetone and ethanol. Working electrodes for SSC were prepared by mixing the CNQ/GH nanocomposite with acetylene black and PVDF in NMP at a mass ratio of 80 : 10 : 10 to form the homogeneous slurry. The resulting slurry was coated on nickel foam substrate and dried at 70 °C for 12 h and then, pressed under a pressure of 10 MPa to form a working electrode. The loading mass of the active material was approximately 0.5 mg cm^{-2}. Then, the prepared two working electrodes were assembled with a polytetrafluoroethylene (PTFE) membrane separator and PVA/KOH gel electrolyte using gentle pressure. The specific capacitance (C_s) of the product was calculated based on the GCD measurements according to the following equation:[28]

$$C_s = \frac{I \times \Delta t}{m \times \Delta V}$$

where I (A), Δt (s), ΔV (V), and m (g) denote the discharge current, discharge time, potential window, and the mass of the active material, respectively. The energy density E (W h kg^{-1}) and power density P (W kg^{-1}) of the device were calculated using the following respective equations:[28]

$$E = \frac{C_s \times (\Delta V)2}{2 \times 3.6}$$

$$P = \frac{3600 \times E}{\Delta t}$$

© 2022 The Author(s). Published by the Royal Society of Chemistry

Open Access Article. Published on 27 January 2022. Downloaded on 2/8/2026 1:35:48 PM.
This article is licensed under a Creative Commons Attribution-NonCommercial 3.0 Unported Licence.

Results and discussion

The schematic of the synthesis of CNQ/GH nanocomposites is illustrated in Fig. 1, where one-pot hydrothermal reaction of the mixture solution of GO and CNQDs was carried out to form CNQDs embedded GH composites. The photograph in Fig. 1 shows a cylindrical sample of the as-prepared CNQ/GH nanocomposite. During the hydrothermal process, GO sheets were stacked and self-assembled into a 3D interconnected hydrogel network with abundant macropores and mesopores. In addition, CNQDs were simultaneously deposited on GO sheets by the π–π interaction on fabricating GH. The surface morphology of CNQ/GH nanocomposite was examined using SEM. As seen in Fig. 2a and b, CNQ/GH nanocomposite exhibits a macroporous morphology with an interconnected 3D network of stacked graphene layers, where abundant well-defined hierarchical macropores and mesopores were observed. In a comparison, CNQ/GH composites possess a similar porous morphology of GH obtained without CNQDs (Fig. S1†). The EDS elemental mapping images in Fig. 2c show a uniform distribution of C, O, and N atoms in the CNQ/GH nanocomposite. The morphology of the CNQ/GH composite was further examined using TEM measurement. It can be seen that CNQDs are embedded in wrinkled graphene sheets (Fig. 2d and e). The HRTEM image of CNQDs on graphene (Fig. 2f) presents an obvious lattice fringe of 0.336 nm corresponding to (002) facet of g-C_3N_4 with a diameter of approximately 3 nm. These results indicate the successful decoration of CNQDs on GH by the one-pot hydrothermal process. Furthermore, the porous structure of GH and CNQ/GH composite was investigated using N_2 adsorption–desorption isotherms as shown in Fig. S2.† The N_2 adsorption isotherms of GH and CNQ/GH show distinct hysteresis loops with a wide pore size distribution, which indicates mesoporous structures. The CNQ/GH nanocomposite has a large specific surface area of 627 $m^2 g^{-1}$, which is slightly smaller than that of GH (660 $m^2 g^{-1}$) due to the deposition of CNQDs on the GH. The large surface area and abundant mesopores of CNQ/GH nanocomposite may hold promise for facilitating efficient electrolyte access and electron transfer for enhanced electrochemical performance.

As shown in Fig. 3a, the XRD pattern of GH shows an intense peak at $2\theta = 25°$ and a small peak at $2\theta = 43°$, corresponding to the (002) and (100) planes of graphite, respectively. In contrast to GH, after fabrication of CNQ/GH nanocomposites, both peaks of (002) and (100) planes become broader and less intense with increasing CNQDs content. The observed change is attributed to the unordered stacking of graphene sheets of GH due to the incorporation of CNQDs 11. Thus, CNQDs can be effectively embedded onto graphene sheets by the π–π interactions between them, which prevent the restacking of graphene sheets during the hydrothermal process, resulting in peak broadening and weakening of the peak intensity of GH. Fig. 3b presents FTIR spectra of the prepared GH and CNQ/GH nanocomposites. All samples exhibit peaks centered at 1217, 1400, and 1720 cm^{-1} corresponding to the stretching vibrations of C–C, C–O–H, and C=O, respectively. In addition, it is worth mentioning that the CNQ/GH nanocomposites exhibit a distinct new peak centered at 1580 cm^{-1}, belonging to the typical stretching vibrations of the C=N band, which is not observed in GH. In addition, Raman spectrum (Fig. S3†) exhibit that the I_d/I_g ratio of graphene increased gradually as the addition of CNQDs. These results suggest that CNQDs are well embedded on graphene sheets to form CNQ/GH nanocomposites.

For further analysis of the surface chemical composition of the CNQ/GH nanocomposite, XPS measurements were performed, and Fig. 4a shows the XPS survey spectra of GH and CNQ/GH nanocomposite. The peaks of C atoms are observed for both samples, whereas the peaks of N are recorded only for CNQ/GH nanocomposite, indicating the presence of CNQDs. In Fig. 4b, the deconvolution of C 1s spectrum for GH exhibits different carbon-containing groups centered at 284.7, 285.3, 286.3, and 288.8 eV, assigning to C–C/C=C in graphene plane, C–OH, C–O and O–C=O bonds, respectively.[29] In comparison to GH, new peaks were observed in the C 1s spectrum of CNQ/GH composite as seen in Fig. 4c, which are centered at 286.3 and 287.4 eV corresponding to C–N/C–O and C=N bonds from CNQDs. Deconvolution of the N 1s spectrum of CNQ/GH reveals three peaks centered at 399.6, 401.1, and 402.7 eV, attributing to pyridinic N, pyrrolic N, and graphitic N, respectively. Of these three nitrogen configurations, pyridinic N and pyrrolic N are expected to contribute to pseudocapacitance through Faraday reactions, whereas graphitic N is considered to increase the conductivity of materials, which could improve the capacitive performance.[30,31] In addition, N in CNQDs can lead the change of electron distribution of graphene, which can improve wettability of electrolyte, resulting in an increase in the accessible surface area to the electrolyte.

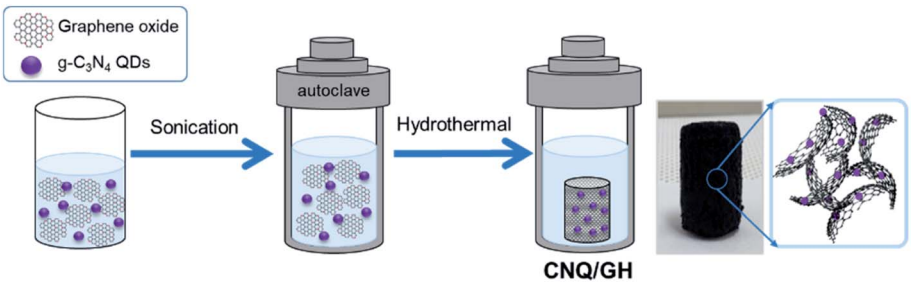

Fig. 1 Schematic illustration of synthesis of CNQ/GH nanocomposites *via* hydrothermal process.

Open Access Article. Published on 27 January 2022. Downloaded on 2/8/2026 1:35:48 PM.
This article is licensed under a Creative Commons Attribution-NonCommercial 3.0 Unported Licence.

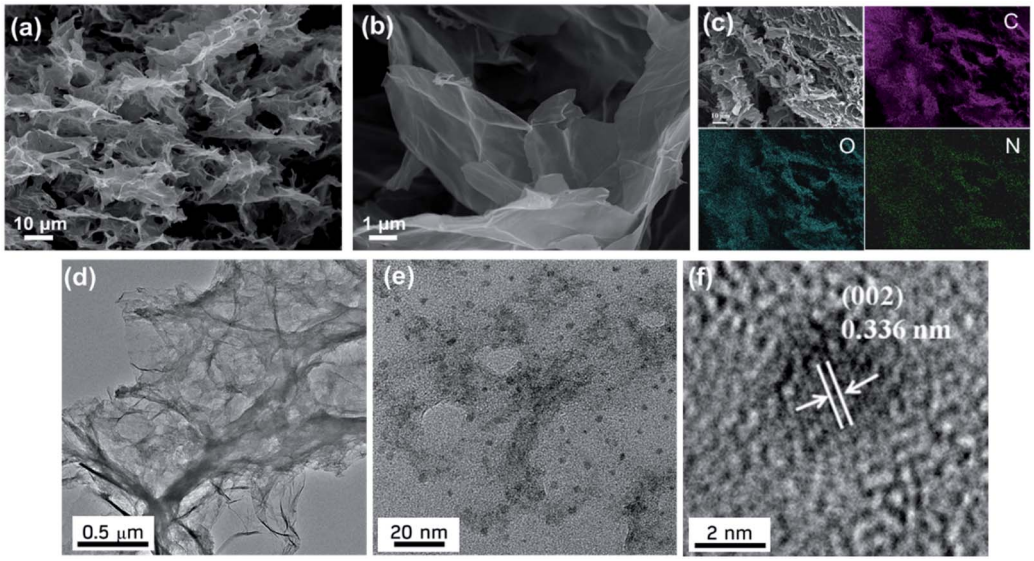

Fig. 2 (a and b) SEM images of CNQ/GH composite and (c) its EDS elemental mapping images. (d and e) TEM images of CNQ/GH composite and (f) its high resolution image.

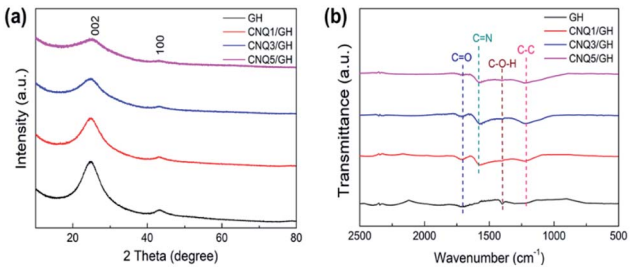

Fig. 3 (a) XRD patterns and (b) FTIR spectra of GH and CNQ/GH nanocomposites.

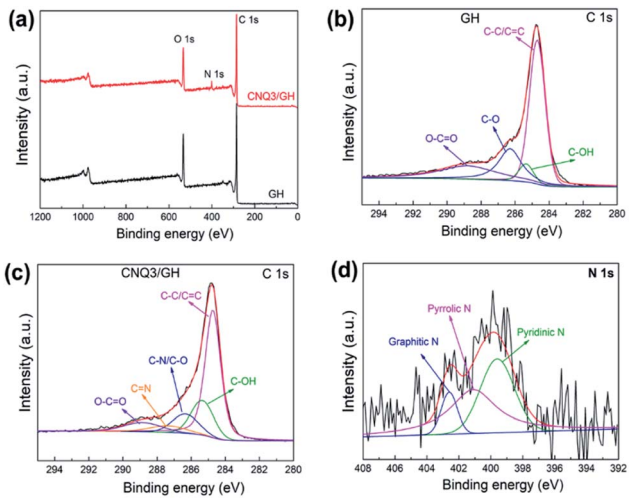

Fig. 4 (a) XPS survey spectra of GH and CNQ3/GH samples. High resolution C 1s spectra of (b) GH and (c) CNQ/GH nanocomposite. (d) High resolution N 1s spectra of CNQ/GH nanocomposite.

The electrochemical performances of the obtained electrode materials for use in supercapacitor were investigated. Cyclic voltammetry (CV), galvanostatic charge/discharge (GCD), and electrochemical impedance spectroscopy (EIS) tests were performed using a three-electrode system in a 6 M aqueous KOH electrolyte. Fig. 5a shows the CV curves of GH and different CNQ/GH electrode obtained at a scan rate of 5 mV s^{-1} over a potential varying from −0.2 to 0.8 V. The CV curves have a distorted rectangular shape for CNQ/GH electrodes, suggesting the electric double layer capacitance and limited pseudocapacitance due to the existence of the CNQDs. It also reveals that the CNQ/GH electrodes exhibit significantly improved capacitive behavior over the GH electrode. The GCD curves of GH and different CNQ/GH electrodes at a current density of 0.2 A g^{-1} are shown in Fig. 5b. The CNQ3/GH nanocomposite shows a much higher specific capacitance, calculated to be 243.2 F g^{-1} compared to GH (53.1 F g^{-1}), confirming the beneficial synergistic effect between CNQDs and GH, which is consistent with the obtained CV results. Fig. 5c presents the CV curves of the CNQ3/GH electrode at different scan rates. The current responses of the CNQ3/GH electrode increase with increasing scan rate, and the CV curves deviate from a distorted rectangular shape to spindle shape at a high scan rate. The GCD curves of the CNQ3/GH electrode were obtained at different current densities, as shown in Fig. 5d. It is found that the specific capacitance decreases with increasing current density due to limited diffusion and transfer of ions as the current density increases. The specific capacitances of the CNQ3/GH electrode were determined to be 243.2 and 201.6 F g^{-1} at current densities of 0.2 and 1.5 A g^{-1}, respectively, which suggests that 83% of its specific capacitance is retained with increasing current density. The change in the observed capacitance of the prepared GH and CNQ/GH electrodes at different current densities is also presented for comparison in Fig. 5e.

© 2022 The Author(s). Published by the Royal Society of Chemistry

Open Access Article. Published on 27 January 2022. Downloaded on 2/8/2026 1:35:48 PM.
This article is licensed under a Creative Commons Attribution-NonCommercial 3.0 Unported Licence.

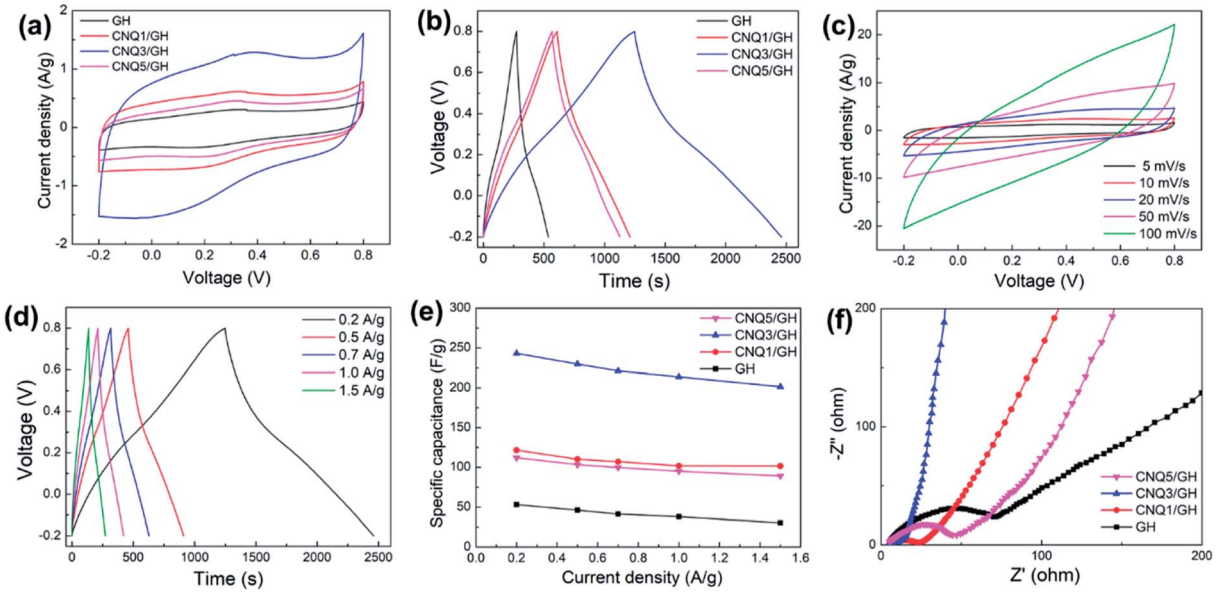

Fig. 5 (a and b) CV curves at a scan rate of 5 mV s^{-1} and GCD curves at 0.2 A g^{-1} of GH and different CNQ/GH nanocomposites, respectively. (c) CV curves of CNQ3/GH nanocomposite at different scan rates from 5 to 100 mV s^{-1} and (d) GCD curves of CNQ3/GH nanocomposite at different current density from 0.2 to 1.5 A g^{-1}. (e) The specific capacitance at different current densities of GH and different CNQ/GH nanocomposites. (f) Electrochemical impedance spectroscopy (EIS) of GH and different CNQ/GH nanocomposites.

The GH electrode retains only 57% of its specific capacitance at the same current density change, decreasing from 53.1 to 30.4 F g^{-1}. It is worth noting that these capacitive performances of the CNQ/GH electrode are substantially higher than or comparable to those of previously reported GH-based electrodes (Table S1†). To further understand the electrochemical kinetics of the CNQ/GH electrode, EIS measurements were carried out over a frequency range from 10 kHz to 0.01 Hz in a 6 M KOH electrolyte. Fig. 5f shows the Nyquist plots of GH and CNQ/GH electrodes with an equivalent circuit, where R_s represents the intrinsic internal resistance in series of the electrochemical system, R_{ct} is the charge-transfer resistance at the electrode–electrolyte contact interface, and Z_w is the Warburg impedance for the diffusion of electrolyte ion in the bulk of electrode. The semicircular diameter lying in high frequency region denotes R_{ct}, in which smaller semicircles of CNQ/GH electrodes reveals higher electrical conductivity than that of GH electrode. The higher slopes of the straight lines in the low-frequency region for the CNQ/GH electrodes also demonstrate a faster ion transfer rates between electrode and electrolyte than that of GH electrode. The CNQ3/GH shows the smallest semicircle diameter and the highest slope of the straight line, which is consistent with the above-mentioned electrochemical performances results. The introduction of CNQDs to GH can not only improve the electrochemical performance but also enhance the cycle stability due to the uniform and homogeneous distribution of CNQDs on the GH surface. However, for the higher amount of CNQDs than CNQ3/GH, the sacrifice of contact area between GH and the electrolyte will happen that leads to a negative effect on the electrode performance. These results imply that the CNQ/GH electrode has enhanced charge-transfer characteristics with fast ion transport and electrolyte diffusion, resulting in improved electrochemical performance due to the beneficial synergistic effect between CNQDs and GH.

To better evaluate the practical performance of CNQ/GH electrodes, all-solid-state symmetric supercapacitors (SSC) were fabricated using two CNQ/GH electrodes as cathode and anode with PVA/KOH gel electrolyte. Fig. 6a shows CV curves of as-fabricated SSC using CNQ/GH electrodes at different scan rates of 5–100 mV s^{-1} with a potential window from 0 to 1.0 V. The CV curves retain a distorted rectangular shape without distinct distortion with increasing scan rates, which indicates the excellent rate capability of the CNQ/GH electrode. The GCD curves of the SSC device using CNQ/GH electrodes at different current densities are shown in Fig. 6b. The estimated specific capacitance is 162.3 F g^{-1} at a current density of 0.5 A g^{-1}. To further evaluate the flexibility of as-prepared SSC with CNQ/GH electrodes, the CV curves were collected under different bending angles at a scan rate of 50 mV s^{-1} (Fig. 6c). The CV shapes were well retained even at a 180° bending angle, which demonstrates good mechanical stability of the SSC with CNQ/GH electrodes. The energy density and power density are considered important parameters for evaluating the electrochemical performance of supercapacitors. The Ragone plots of the SSC with CNQ/GH electrodes are shown in Fig. 6d with the results of previously reported graphene-based SSCs. It is obviously observed that the SSC fabricated with CNQ/GH electrode delivers a high energy density of 22.5 W h kg^{-1} at a power density of 250 W kg^{-1} and retains 4.6 W h kg^{-1} at a high power density of 2500 W kg^{-1}. These performances are superior to those of other reported electrodes including N,S co-doped GH (6.25 W h kg^{-1} at a power density of 500 W kg^{-1}),[32] N,S co-doped graphene (8.3 W h kg^{-1} at a power density of 510 W kg^{-1}),[33] N,S co-doped carbon spheres (18.1 W h kg^{-1} at a power density of

Open Access Article. Published on 27 January 2022. Downloaded on 2/8/2026 1:35:48 PM.
This article is licensed under a Creative Commons Attribution-NonCommercial 3.0 Unported Licence.

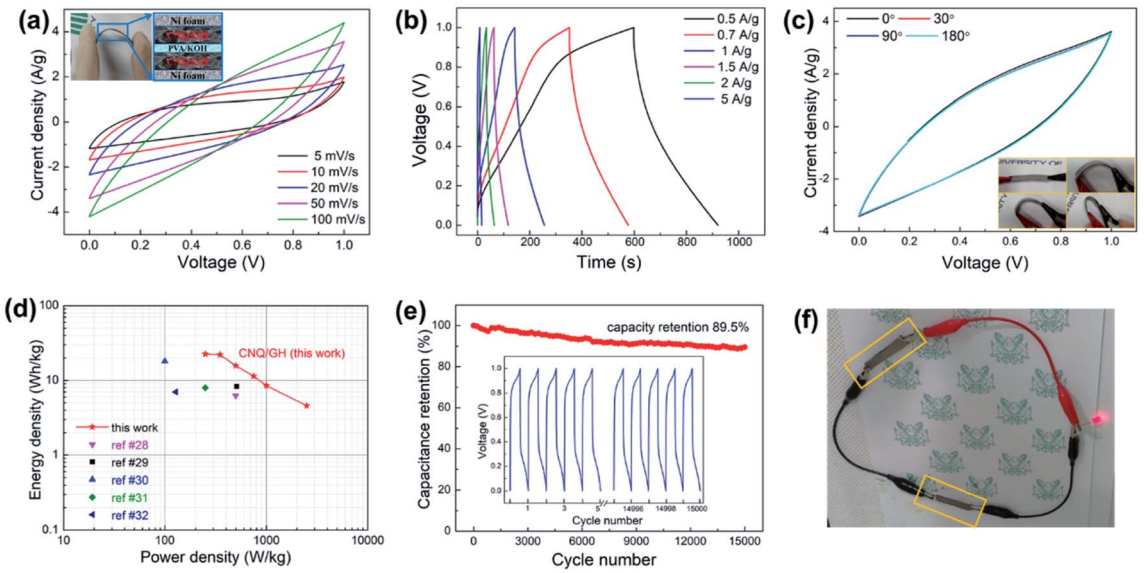

Fig. 6 (a) CV curves of the SSC device using CNQ3/GH electrodes at various scan rates from 5 to 100 mV s^{-1} (inset is the photograph of device). (b) GCD curves of the SSC at different current density from 0.5 to 5 A g^{-1}. (c) CV curves of the device under different bending conditions at a scan rate of 50 mV s^{-1} (inset is photographs of the SSC under different bending conditions). (d) Ragone plots of the SSC of CNQ3/GH electrode and their comparison with the reported values. (e) Cycling stabilities of the SSC of CNQ3/GH electrodes over 15 000 cycles at a current density of 5 A g^{-1} (inset is the GCD curves from 1st to 5th cycles and from 14995th to 15000th cycles). (f) The photograph of two SSC devices with CNQ3/GH electrodes connected in series lighting the red LED.

100 W kg^{-1}),[34] N,F co-doped GH (7.99 W h kg^{-1} at a power density of 250 W kg^{-1}),[35] and N-doped porous carbon nanosheets (7.0 W h kg^{-1} at power density of 128 W kg^{-1}).[36] In addition, the long-term cycling stability of the SSC with CQD/GH electrodes was studied by charge–discharge tests at a current density of 5 A g^{-1} as shown in Fig. 6e. The GCD curves of the SSC with CNQ/GH electrodes from 1st to 5th cycle and from the 14 995th to 15 000th cycles are shown in the inset of Fig. 6e, where only slight change in the GCD curves is observed. The cycle stability still retains 89.5% of the initial capacitance after 15 000 cycles, indicating its excellent long-term cycling stability. Furthermore, two SSC devices with CNQ/GH electrodes connected in series can power a commercial red light-emitting diode (LED), showing its potential for practical applications (Fig. 6f). These excellent capacitive performances of CNQ/GH electrodes are attributed to the highly porous structure of the electrodes and the synergistic effect of CNQDs and GH nanocomposites. The large surface area and mesoporosity of the CNQ/GH electrode provide effective contact between the electrode and the electrolyte and a short diffusion distance, which facilitates fast ion diffusion of electrode. In addition, the various C–N bonds in CNQDs can serve as active sites for pseudocapacitance through faradaic reactions with increased electrical conductivity and better wettability of electrolyte.

Conclusions

In summary, the CNQ/GH nanocomposites were prepared using a simple one-pot hydrothermal process, in which CNQDs were embedded onto the graphene surface of porous GH. The introduction of CNQDs into the GH leads to an increase in pseudocapacitive activity and electrical conductivity, and the highly porous GH promotes an efficient contact of the electrolyte with the electrodes, demonstrating the excellent performance for supercapacitor applications. The prepared CNQ3/GH electrode exhibits high specific capacitance of 243.2 F g^{-1} at a current density of 0.2 A g^{-1} with better rate capability. The CNQ3/GH composite might form the optimal coverage of CNQDs on GH surface for better electrochemical performance. Furthermore, the flexible SSC devices fabricated using CNQ/GH electrodes deliver a high energy density of 22.5 W h kg^{-1} at a power density of 250 W kg^{-1} and excellent cycling stability with capacitance retention of 89.5% after 15 000 cycles. This work would provide an efficient route to develop carbon-based active materials demonstrating potential not only for high-performance supercapacitors but also for other areas such as electrocatalyst and Li-ion batteries.

Conflicts of interest

There are no conflicts to declare.

Acknowledgements

This work was supported by the 2021 Research Fund of the University of Ulsan.

References

1 K. Sharma, A. Arora and S. Tripathi, Review of supercapacitors: materials and devices, *J. Energy Storage*, 2019, **21**, 801–825.

© 2022 The Author(s). Published by the Royal Society of Chemistry

Open Access Article. Published on 27 January 2022. Downloaded on 2/8/2026 1:35:48 PM.
This article is licensed under a Creative Commons Attribution-NonCommercial 3.0 Unported Licence.

2 A. González, E. Goikolea, J. A. Barrena and R. Mysyk, Review on supercapacitors: technologies and materials, *Renewable Sustainable Energy Rev.*, 2016, **58**, 1189–1206.
3 L. Zhang, W.-B. Zhang, S.-S. Chai, X.-W. Han, Q. Zhang, X. Bao, Y.-W. Guo, X.-L. Zhang, X. Zhou, S.-B. Guo and X.-J. Ma, Review—clay mineral materials for electrochemical capacitance application, *J. Electrochem. Soc.*, 2021, **168**, 070558.
4 G. Wang, L. Zhang and J. Zhang, A review of electrode materials for electrochemical supercapacitors, *Chem. Soc. Rev.*, 2012, **41**, 797–828.
5 A. Borenstein, O. Hanna, R. Attias, S. Luski, T. Brousse and D. Aurbach, Carbon-based composite materials for supercapacitor electrodes: a review, *J. Mater. Chem. A*, 2017, **5**, 12653–12672.
6 L. L. Zhang and X. S. Zhao, Carbon-based materials as supercapacitor electrodes, *Chem. Soc. Rev.*, 2009, **38**, 2520–2531.
7 S.-M. Chen, R. Ramachandran, V. Mani and R. Saraswathi, Recent advancements in electrode materials for the high-performance electrochemical supercapacitors: a review, *Int. J. Electrochem. Sci.*, 2014, **9**, 4072–4085.
8 M. Shang, X. Zhang, J. Zhang, J. Sun, X. Zhao, S. Yu, X. Liu, B. Liu and X. Yi, Nitrogen-doped carbon composite derived from ZIF-8/polyaniline@cellulose-derived carbon aerogel for high-performance symmetric supercapacitors, *Carbohydr. Polym.*, 2021, **262**, 117966.
9 M. Wang, J. Zhang, X. Yi, X. Zhao, B. Liu and X. Liu, Nitrogen-doped hierarchical porous carbon derived from ZIF-8 supported on carbon aerogels with advanced performance for supercapacitor, *Appl. Surf. Sci.*, 2020, **507**, 145166.
10 R. Dubey and V. Guruviah, Review of carbon-based electrode materials for supercapacitor energy storage, *Ionics*, 2019, **25**, 1419–1445.
11 Q. Ke and J. Wang, Graphene-based materials for supercapacitor electrodes–a review, *J. Mater.*, 2016, **2**, 37–54.
12 W. K. Chee, H. N. Lim, Z. Zainal, N. M. Huang, I. Harrison and Y. Andou, Flexible graphene-based supercapacitors: a review, *J. Phys. Chem. C*, 2016, **120**, 4153–4172.
13 A. S. Lemine, M. M. Zagho, T. M. Altahtamouni and N. Bensalah, Graphene a promising electrode material for supercapacitors—a review, *Int. J. Energy Res.*, 2018, **42**, 4284–4300.
14 Y. Xu, Z. Lin, X. Huang, Y. Wang, Y. Huang and X. Duan, Functionalized graphene hydrogel-based high-performance supercapacitors, *Adv. Mater.*, 2013, **25**, 5779–5784.
15 Y. Xu, Z. Lin, X. Huang, Y. Liu, Y. Huang and X. Duan, Flexible solid-state supercapacitors based on three-dimensional graphene hydrogel films, *ACS Nano*, 2013, **7**, 4042–4049.
16 A. Khazaei, G. Godbille-Cardona and D. P. J. Barz, A novel flexible hybrid battery- supercapacitor based on a self-assembled vanadium-graphene hydrogel, *Adv. Funct. Mater.*, 2020, **30**, 1910738.
17 R. Lin, Z. Li, D. I. A. El Amaiem, B. Zhang, D. J. Brett, G. He and I. P. Parkin, A general method for boosting the supercapacitor performance of graphitic carbon nitride/graphene hybrids, *J. Mater. Chem.*, 2017, **5**, 25545–25554.
18 M. Ashritha and K. Hareesh, A review on graphitic carbon nitride based binary nanocomposites as supercapacitors, *J. Energy Storage*, 2020, **32**, 101840.
19 B. T. Dong, M. Y. Li, S. Chen, D. W. Ding, W. Wei, G. X. Gao and S. J. Ding, Formation of g-C_3N_4@Ni$(OH)_2$ honeycomb nanostructure and asymmetric supercapacitor with high energy and power density, *ACS Appl. Mater. Interfaces*, 2017, **9**, 17890–17896.
20 M. Ghaemmaghami and R. Mohanmmadi, Carbon nitride as a new way to facilitate the next generation of carbon-based supercapacitors, *Sustainable Energy Fuels*, 2019, **3**, 2176–2204.
21 Z. Lin, K. Wang, X. Wang, S. Wang, H. Pan, Y. Liu, S. Xu and S. Cao, Carbon-coated graphitic carbon nitride nanotubes for supercapacitor applications, *ACS Appl. Mater. Interfaces*, 2020, **3**, 7016–7028.
22 J. Safaei, N. A. Mohamed, M. F. Mohamad Noh, M. F. Soh, N. A. Ludin, M. A. Ibrahim, W. N. Roslam Wan Isahak and M. A. Mat Teridi, Graphitic carbon nitride (g-C_3N_4) electrodes for energy conversion and storage: a review on photoelectrochemical water splitting, solar cells and supercapacitors, *J. Mater. Chem. A*, 2018, **6**, 22346–22380.
23 Q. Chen, Y. Zhao, X. K. Huang, N. Chen and L. T. Qu, Three-dimensional graphitic carbon nitride functionalized graphene-based high-performance supercapacitors, *J. Mater. Chem. A*, 2015, **3**, 6761–6766.
24 Y. Liao, Y. Huang, D. Shu, Y. Zhong, J. Hao, C. He, J. Zhong and X. Song, Three-dimensional nitrogen-doped graphene hydrogels prepared via hydrothermal synthesis as high-performance supercapacitor materials, *Electrochim. Acta*, 2016, **194**, 136–142.
25 Z. Li, J. Wei, J. Ren, X. Wu, L. Wang, D. Pan and M. Wu, Hierarchical construction of high-performance all-carbon flexible fiber supercapacitors with graphene hydrogel and nitrogen-doped graphene quantum dots, *Carbon*, 2019, **154**, 410–419.
26 D. Liu, S. H. Hur, J. S. Chung and W. M. Choi, Fabrication of g-C_3N_4 quantum dots/$MnCO_3$ nanocomposite on carbon cloth for flexible supercapacitor electrode, *Appl. Sci.*, 2020, **10**, 7927.
27 T. V. Tam, S. G. Kang, K. F. Babu, E.-S. Oh, S. G. Lee and W. M. Choi, Synthesis of B-doped graphene quantum dots as a metal-free electrocatalyst for the oxygen reduction reaction, *J. Mater. Chem. A*, 2017, **5**, 10537–10543.
28 H. Li, Z. Li, M. Sun, Z. Wu, W. Shen and Y. Q. Fu, Zinc cobalt sulfide nanoparticles as high performance electrode material for asymmetric supercapacitor, *Electrochim. Acta*, 2019, **319**, 716–726.
29 W. Zhou, S. Lei, S. Sun, X. Ou, Q. Fu, Y. Xu, Y. Xiao and B. Cheng, From weed to multi-heteroatom-doped honeycomb-like porous carbon for advanced supercapacitors: a gelatinization-controlled one-step carbonization, *J. Power Sources*, 2018, **402**, 203–212.
30 S. G. Dai, Z. Liu, B. T. Zhao, J. H. Zeng, H. Hu, Q. B. Zhang, D. C. Chen, C. Qu, D. Dang and M. L. Liu, A high-

Open Access Article. Published on 27 January 2022. Downloaded on 2/8/2026 1:35:48 PM.
This article is licensed under a Creative Commons Attribution-NonCommercial 3.0 Unported Licence.

performance supercapacitor electrode based on N-doped porous graphene, *J. Power Sources*, 2018, **387**, 43–48.

31 Y. Q. Zou, I. A. Kinloch and R. A. W. Dryfe, Nitrogen-doped and crumpled graphene sheets with improved supercapacitance, *J. Mater. Chem. A*, 2014, **2**, 19495–19499.

32 W. J. Zhang, Z. T. Chen, X. L. Guo, K. Jin, Y. X. Wang, L. Li, Y. Zhang, Z. M. Wang, L. T. Sun and T. Zhang, N/S co-doped three-dimensional graphene hydrogel for high performance supercapacitor, *Electrochim. Acta*, 2018, **278**, 51–60.

33 L. Cheng, Y. Hu, D. Qiao, Y. Zhu, H. Wang and Z. Jiao, One-step radiolytic synthesis of heteroatom (N and S) co-doped graphene for supercapacitors, *Electrochim. Acta*, 2018, **259**, 587–597.

34 G. Xin, M. Wang, W. Zhang, J. Song and B. Zhang, Preparation of high-capacitance N, S co-doped carbon nanospheres with hierarchical pores as supercapacitors, *Electrochim. Acta*, 2018, **291**, 168–176.

35 Y. Chen, Y. Li, F. Yao, C. Peng, C. Cao, Y. Feng and W. Feng, Nitrogen and fluorine co-doped holey graphene hydrogel as a binder-free electrode material for flexible solid-state supercapacitors, *Sustainable Energy Fuels*, 2019, **3**, 2237–2245.

36 M. Wang, J. Yang, S. Liu, M. Li, C. Hu and J. Qiu, Nitrogen-doped hierarchically porous carbon nanosheets derived from polymer/graphene oxide hydrogels for high-performance supercapacitors, *J. Colloid Interface Sci.*, 2020, **560**, 69–76.

© 2022 The Author(s). Published by the Royal Society of Chemistry